Advances in Geo-Energy Research

Vol. 16, No. 3, p. 276-287, 2025

Original article

Addressing mobility control challenges in high-pressure high-temperature oil reservoirs via water-saturated CO_2 injection

Hang Yin[1], Jiachao Ge[1,2,3], Furqan Hussain[1]*

[1]School of Minerals and Energy Resources Engineering, University of New South Wales, Sydney, NSW 2052, Australia

[2]State Key Laboratory of Offshore Oil and Gas Exploitation, Beijing 102209, P. R. China

[3]CNOOC Research Institute, Beijing 100028, P. R. China

Keywords:
Water-saturated CO_2 injection
mobility control
high-temperature
CO_2 storage
field-scale simulation

Cited as:
Yin, H., Ge, J., Hussain, F. Addressing mobility control challenges in high-pressure high-temperature oil reservoirs via water-saturated CO_2 injection. Advances in Geo-Energy Research, 2025, 16(3): 276-287.
https://doi.org/10.46690/ager.2025.06.07

Abstract:
The ability of pure CO_2 injection into an oil reservoir to bring about CO_2 storage is hindered by the fact that CO_2 is more mobile than oil. Most "mobility control" methods (such as foam injection) work only at low temperatures. This study investigates whether water-saturated CO_2 injection can provide mobility control at high pressures and temperatures. In this study, CO_2 and water-saturated CO_2 are injected into a Bentheimer sandstone core. Experimental runs are performed at 70 °C to simulate a low-temperature reservoir and 116 °C to simulate a high-temperature reservoir. The selected pressure ranges from 10.3 to 18.6 MPa. Results show that water-saturated CO_2 consistently exhibits lower mobility than pure CO_2. Hence, water-saturated CO_2 injection provides effective mobility control for both low- and high-temperature reservoirs, especially at higher pressure. The effectiveness of water-saturated CO_2 in reducing mobility compared to pure CO_2 increases exponentially with pressure. Despite the improved mobility control provided by water-saturated CO_2 injection, experimental observation finds net CO_2 stored and oil recovery to be similar to that of pure CO_2 injection, as CO_2 sweep efficiency is already high in experimental runs. However, at field-scale sweep efficiency is low. Therefore, field-scale simulations reveal a 19%-47% increase in net CO_2 stored during water-saturated CO_2 injection compared to pure CO_2 injection.

1. Introduction

In CO_2 enhanced oil recovery (CO_2-EOR) projects, both oil recovery and CO_2 storage are often constrained by unfavourable mobility ratio – defined as the ratio between the mobility of CO_2 and that of oil – which causes a poor CO_2 sweep efficiency (Liu et al., 2011; Kim and Santamarina, 2014; Zhao et al., 2015). Mobility ratio indicates the stability of the displacement front for CO_2 injection. Mobility ratio more than 1 represents the displacing fluid has a larger mobility than the displaced fluid, thus leading to poor sweep efficiency displacement. In contrast, a mobility ratio of nearly or lower than 1 indicates high sweep efficiency. Mobility control refers to modifying the mobility ratio between the displacing fluid (e.g., CO_2) and the displaced fluid (e.g., oil) to achieve more efficient displacement (Lake, 1989). This is often done by reducing the mobility of the displacing fluid to prevent it from bypassing large volumes of the reservoir and thus improving sweep efficiency and oil recovery. Typical mobility control methods include CO_2 water alternating gas (CO_2-WAG) injection (Kumar and Mandal, 2017), CO_2 simultaneous water and gas (CO_2-SWAG) injection (Kamali et al., 2017),

*Corresponding author.
E-mail address: hang.yin1@unsw.edu.au (H. Yin); gejch3@cnooc.com.cn (J. Ge); furqan.hussain@unsw.edu.au (F. Hussain).

Yandy Scientific Press

2207-9963
Received April 7, 2025; revised May 6, 2025; accepted May 21, 2025; available online May 26, 2025.

and CO_2-foam injection (Zhou et al., 2024). However, these approaches often face challenges, such as reduced CO_2 storage capacity and limited applicability under high-pressure high-temperature reservoir conditions.

Water injected by CO_2-WAG injection or CO_2-SWAG injection occupies pores that might have been available for CO_2 storage (Kulkarni and Rao, 2005). This makes CO_2-WAG and CO_2-SWAG injection suboptimal CO_2-EOR methods. Foam-based mobility control methods also face limitations. The stability of CO_2-foam is affected by reservoir temperature (Emrani and Nasr-El-Din, 2017; Chen et al., 2025), and many reservoirs have high temperatures, usually ranging from 70 °C to more than 120 °C (Puerto et al., 2011). To improve stability, agents need to be added to the CO_2-foam (Abdelaal et al., 2020), which increases CO_2-EOR costs (Cao et al., 2020). As summarized in Table S1 in Supplementary file, although various foam agents and thickeners have been tested, CO_2-foam stability generally decreases with increasing temperature, particularly above 70 °C. The long operating life of EOR projects is also constrained by the instability of CO_2-foam injection (Chen et al., 2016). In addition, injecting certain surfactants and nanoparticles as foaming agents during CO_2 foam injection often results in pollution to the environment and the formation (Lv et al., 2023). Clark and Santiso (2018) illustrated that anionic surfactants, nonionic surfactants, and nanoparticles exhibit significant environmental and cytotoxicity toxicity, particularly when large quantities are released into the environment.

wsCO_2 injection is a greener mobility control method, where CO_2 is modified with only water. Its first application in EOR was demonstrated and reported by Ajoma et al. (2020), who visualized water condensation during wsCO_2 interaction with oil. Ajoma et al. (2021a) reported that wsCO_2 injection led to a greater reduction in mobility ratio under miscible conditions, while the effect was negligible under immiscible conditions. To investigate miscibility effects, they varied pressure while maintaining a constant temperature. The improvements in oil recovery and CO_2 storage were more pronounced at lower injection rates. Ajoma et al. (2021b) experimentally compared wsCO_2 injection with CO_2-SWAG injection. Results showed that wsCO_2 injection achieved comparable oil recovery to CO_2-SWAG injection while enabling 22% greater CO_2 storage, highlighting its potential for enhancing CO_2 storage efficiency in CO_2-EOR projects. Yin et al. (2023) studied the impact of gravity on wsCO_2 injection and found that CO_2 storage and tertiary oil recovery improved when the adverse gravitational effect caused low sweep efficiency. Yin et al. (2025) studied the impact of pore heterogeneity on wsCO_2 injection and found that wsCO_2 could enter pores up to 10 times smaller than those accessed by pure CO_2 injection. The mechanism of wsCO_2 injection can be summarized as follows: Initially, wsCO_2 contacts oil in an immiscible manner, similar to pure CO_2 (Perera et al., 2016). Subsequently, mass transfer occurs at the CO_2-oil interface, where the CO_2 component of wsCO_2 condenses into the oil-rich phase (condensation drive) while lighter oil components vaporize into the CO_2-rich phase (vaporization drive) (Kumar et al., 2022). After multiple contacts, a miscible bank is formed (Arshad et al., 2009). Unlike pure CO_2, wsCO_2 injection can lead to emulsification due to water condensing into the oil phase, resulting in high-viscosity emulsions that increase flow resistance and pressure difference (Yin et al., 2025).

This study aims to evaluate the effectiveness of wsCO_2 injection for mobility control across a range of pressure and temperature conditions. By examining its performance under varying reservoir conditions, this method extends its applicability to a broader spectrum of oil fields, particularly those with high temperatures. It offers a practical and sustainable approach to enhancing CO_2 storage strategies in such reservoirs.

2. Materials and methods

2.1 Rock and fluids

A cylindrical Bentheimer sandstone core sample, with a length of 138 mm and a diameter of 38 mm, was used in this study. This core sample is hereafter referred to as the "core" for simplicity. The core had permeability 1.2 D and porosity 24.5%. Bentheimer sandstone was selected due to its homogeneous pore structure and widespread use in similar studies involving CO_2 injection (Zou et al., 2018; Ajoma et al., 2020). To ensure consistency and comparability, the same rock type was adopted in this study. Detailed characterization of the rock has been provided by Yin et al. (2025).

MilliQ^{TM} water was used as the water phase. Light crude oil was used as the oil phase, and 116 °C and 15.5 MPa represent the conditions of the reservoir where the crude oil was obtained. Pure CO_2 and wsCO_2 were used for CO_2 injection. Table 1 summarizes the fluid properties used.

2.2 Experimental setup and procedure

2.2.1 IFT measurement

Interfacial Tension (IFT) was measured using the capillary rise method in a high-pressure high-temperature cell (Saira et al., 2020b, 2021b). CO_2-oil capillary rise images were captured and analyzed using ImageJ software (Schneider et al., 2012) to determine IFT.

2.2.2 Injection experiment

The experimental setup used by Yin et al. (2025) was modified to perform high temperature experiments (Fig. 1). High-temperature components (OMEGA heating tapes, RS temperature controllers, and glass fiber insulation) were used to further increase the temperature to 116 °C and maintain it. The high-temperature components were also used at 70 °C to ensure that the experimental runs were comparable.

The preparation of wsCO_2 involves equilibrating CO_2 and water in a 550 cc accumulator. The procedure for an injection experiment is outlined as follows: The core was first saturated with MilliQ^{TM} water then mounted in the core holder. The core holder's temperature was then adjusted to maintain a consistent temperature of either 70 or 116 °C by the temperature controllers. The saturated core then received a 3.8 cc/min oil injection to achieve the irreducible water saturation (S_{wi}), followed by 8 Pore Volume Injected (PVI) of either pure

Table 1. Properties of fluids at different experimental conditions.

Fulid type	Property	Experimental conditions					Calculation method
		70 °C 10.3 MPa	70 °C 12 MPa	116 °C 10.3 MPa	116 °C 14.6 MPa	116 °C 18.6 MPa	
Oil	Density (g/cm^3)	0.740	0.714	0.711	0.716	0.720	CMG-WINPROP (2018)
	Viscosity (cp)	0.702	0.717	0.474	0.505	0.532	
Water	Density (g/cm^3)	0.996	0.996	0.965	0.946	0.965	El-Dessouky (2002)
	Viscosity (cp)	0.429	0.429	0.246	0.240	0.257	
Pure CO_2	Density (g/cm^3)	0.266	0.345	0.180	0.277	0.371	CMG-WINPROP (2018)
	Viscosity (cp)	0.025	0.029	0.024	0.027	0.033	
wsCO_2	Density (g/cm^3)	0.270	0.351	0.190	0.282	0.378	Mass fractions
	Viscosity (cp)	0.028	0.032	0.035	0.038	0.043	Bloomfield and Dewan (1971)
wsCO_2	Water fraction (%mol)	0.69	0.73	2.91	2.70	2.71	CMG-WINPROP (2018)
	Water fraction (%wt)	0.29	0.30	1.21	1.12	1.13	
	Water fraction (%vol)	0.08	0.10	0.23	0.32	0.43	
CO_2-oil	IFT (mN/m)	2.6	0.6	5.5	2.6	0.6	Section 2.3
	Miscibility	Immiscible	Near-miscible	Immiscible	Immiscible	Near-miscible	

Notes: Oil composition provided by Ge et al. (2022) was used to calculate oil properties. The last column indicates the method used to obtain the reported values.

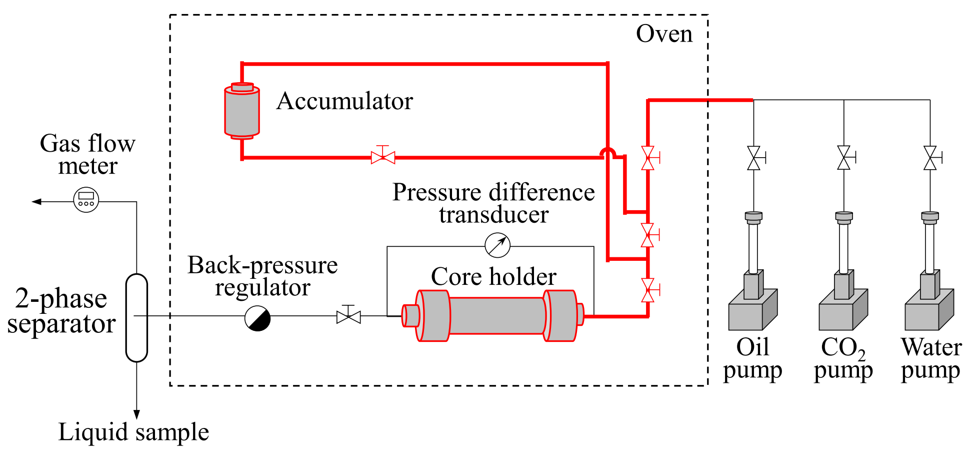

Fig. 1. Schematic of the setup for the injection experiment. The temperature of the fluid path from just outlet of pumps through the core holder was controlled by heating tapes, temperature controllers, and glass fiber insulation (in red). The setup was adapted from Yin et al. (2025).

CO_2 or wsCO_2. The CO_2 injection rate was set to 0.5 cc/min, based on the criteria proposed by Zhou et al. (1994), which involve two numbers: The effective aspect ratio (R_1^2) defined by Eq. (1), and the gravity number (N_g) defined by Eq. (2). In this study, R_1^2 was 13 for all injection experiments, with N_g ranging from 0.7 to 2.6 for pure CO_2 injection and from 0.4 to 2.5 for wsCO_2 injection. The criteria suggest that the experimental conditions in this study exhibit viscous-gravity transition flow regime (Zhou et al., 1994). As most field-scale CO_2 injections are carried out under gravity dominant or viscous-gravity transition regime (Zhou et al., 1994), the conducted experiments fairly depict field conditions. The flow regime is calculated by:

$$R_l^2 = \frac{L^2 k_{av}}{H^2 k_{ah}} \tag{1}$$

$$N_g = N_{gv} M \tag{2}$$

where L is the length of the core for injection experiment or x or y dimension of the grid for field-scale simulation, H is the diameter of the core for injection experiment or

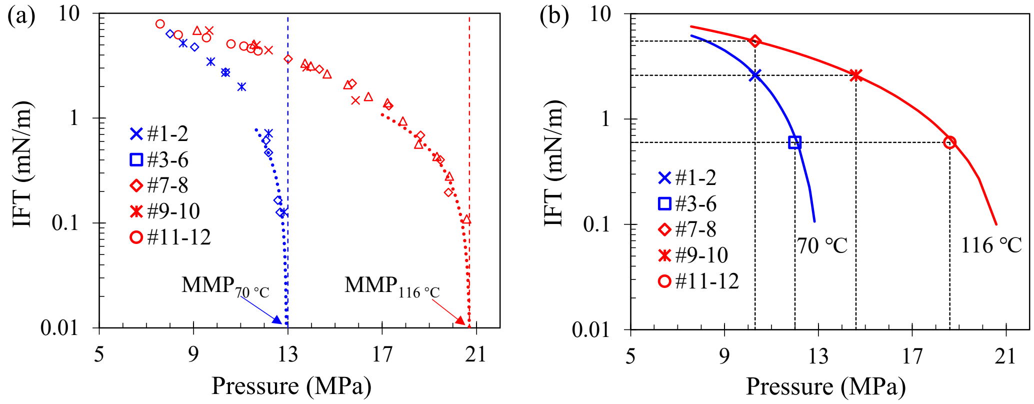

Fig. 2. (a) Experimentally measured IFT at different temperature. Dotted extrapolation lines represent linear fits to estimate MMP and (b) experimental pressures selected for this study: 10.3 and 12 MPa at 70 °C; 10.3, 14.6, and 18.6 MPa at 116 °C.

thickness for field-scale simulation, k_{av} is the average vertical permeability, and k_{ah} is the average horizontal permeability, N_{gv} is the transverse gravity number, and M is the ultimate mobility ratio. N_{gv} and M are defined by:

$$N_{gv} = \frac{\Delta\rho g L k_{av}}{H v \mu_o} \tag{3}$$

$$M = \frac{q_{CO_2}/\Delta P_{CO_2}}{q_o/\Delta P_o} \tag{4}$$

where $\Delta\rho$ is the density difference between oil phase and CO_2 phase, g is the gravity acceleration, v is the displacement velocity, μ_o is the oil viscosity, q_{CO_2} is CO_2 injection rate, ΔP_{CO_2} is ultimate pressure difference across the core at the end of CO_2 injection, q_o is oil injection rate before CO_2 injection, and ΔP_o is ultimate pressure difference across the core during oil injection but before CO_2 injection.

An alternative expression for the M is obtained by applying Darcy's law to Eq. (4), as shown in:

$$M = \frac{k^m_{rCO_2}/\mu_{CO_2}}{k^m_{ro}/\mu_o} \tag{5}$$

where $k^m_{rCO_2}$ is CO_2 endpoint relative permeability, k^m_{ro} is oil endpoint relative permeability, and μ_{CO_2} is the CO_2 viscosity.

Subsequent to the experimental runs, this study processed the obtained experimental data such as pressure difference, oil production, and gas production flow rate. Then, oil recovery (RF) was calculated by:

$$\mathrm{RF} = \frac{N_p}{\mathrm{OIP}} \tag{6}$$

where N_p is cumulated oil produced at reservoir conditions, and OIP is the initial volume of oil in the core.

In addition, net CO_2 stored (NS) was calculated as follows:

$$\mathrm{NS} = \frac{V^I_{CO_2} - V^P_{CO_2}}{\mathrm{PV}} \tag{7}$$

where $V^I_{CO_2}$ is volume of CO_2 injected at experimental conditions, $V^P_{CO_2}$ is volume of CO_2 produced at experimental conditions, and PV is the pore volume of the core.

2.3 Experimental conditions and experimental runs

Two temperatures were selected: 70 °C based on (Kamali et al., 2017) and 116 °C based on actual oil field temperature (Ge et al., 2022). Literature characterizes the temperature of low-temperature oil reservoirs in the range 30-70 °C (Grabowski et al., 2005), and high-temperature oil reservoirs in the range 70-120 °C (Bello et al., 2022). The experimental pressures were selected to represent different levels of miscibility, which were determined by the IFT values observed in this study. IFT measurement runs in this study compared IFT results at different temperatures (Fig. 2(a)). The Vanishing Interfacial Technique (VIT) was used to estimate Minimum Miscibility Pressure (MMP) (Saira et al., 2020a). Using the linear extrapolation of low IFT data (from values around 1 mN/m to values below 0.01 mN/m), the x-axis value at IFT = zero was deemed as the MMP. The estimated MMP values were 13 MPa at 70 °C and 20.7 MPa at 116 °C. Although MMP predicted by VIT method might be erroneous (Orr and Jessen, 2007), it nonetheless provides a useful indicator of whether the system is near-miscible or immiscible.

Thomas et al. (1994) suggested that an IFT at or below 1 mN/m indicates near-miscibility, whereas a value above 1 mN/m indicates immiscibility. Near-miscible pressure is deemed to be 90%-95% of MMP (Shyeh-Yung, 1991). Based on the criteria of Thomas et al. (1994) and Shyeh-Yung (1991), the experimental runs present immiscibility and near-miscibility. Experimental pressures selected for this study are presented in Fig. 2(b).

3. Results and discussion

Table 2 shows that S_{wi} values for all experiments were comparable before CO_2 injection. Experimental Runs #3 and #4 were conducted to assess the reproducibility of pure CO_2 injection. The largest discrepancies between ultimate values in the "mated" experimental runs are a difference in pressure difference of 0.04 kPa, in net CO_2 stored of 2.4%, and in oil recovery of 1.3%. Experimental Runs #5 and #6 were conducted to assess the reproducibility of wsCO_2 injection, resulting in a pressure difference of 0.41 kPa, in net CO_2 stored

Table 2. Result of injection runs.

ID	Temperature (°C)	Pressure (MPa)	Miscibility condition	S_{wi}	Injection fluid	Ultimate ΔP (kPa)	Ultimate NS (ResVol/PV, %)	Ultimate RF (OIP, %)	M
1	70	10.3 (79% MMP)	Immiscible	0.217	Pure CO_2	2.15	38.8	49.7	0.47
2				0.204	wsCO_2	7.12	43.9	55.2	0.24
3	70	12 (94% MMP)	Near-miscible	0.210	Pure CO_2	0.12	56.7	71.8	7.8
4				0.162	Pure CO_2	0.16	59.1	72.4	6.0
5				0.210	wsCO_2	0.85	58.2	73.4	1.1
6				0.167	wsCO_2	0.46	57.0	68.5	1.4
7	116	10.3 (50% MMP)	Immiscible	0.217	Pure CO_2	0.41	32.8	42.0	2.4
8				0.178	wsCO_2	0.49	38.4	46.7	2
9	116	14.6 (71% MMP)	Immiscible	0.168	Pure CO_2	0.22	50.4	59.6	3.8
10				0.173	wsCO_2	0.69	49.0	59.3	1.2
11	116	18.6 (90% MMP)	Near-miscible	0.225	Pure CO_2	0.15	73.6	94.9	6.8
12				0.231	wsCO_2	1.15	71.0	92.2	0.9

Notes: Experimental Runs #4 and #6 were repeat runs of Experimental Runs #3 and #5, respectively, and are excluded from further discussion.

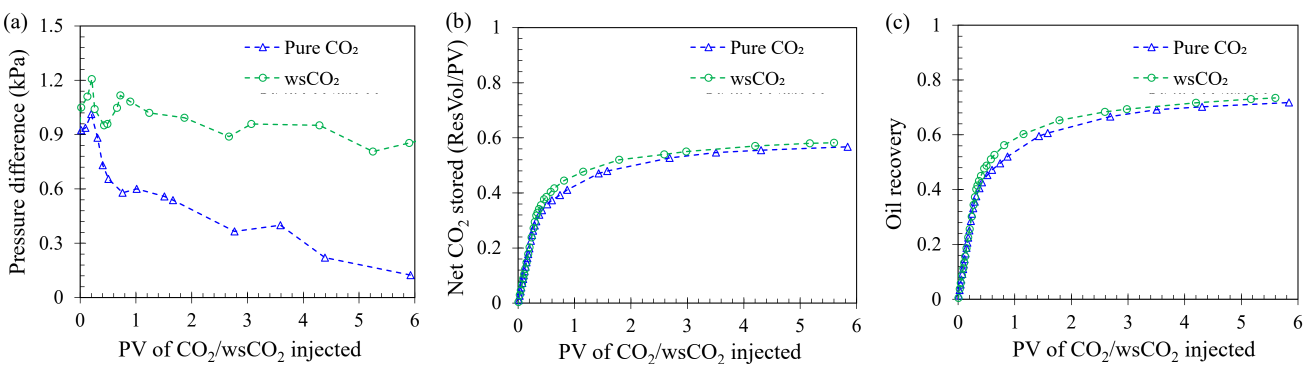

Fig. 3. Comparison of the effects of pure CO_2 (Experimental Run #3) and wsCO_2 (Experimental Run #5) on (a) pressure difference, (b) net CO_2 stored and (c) oil recovery at 70 °C and 12 MPa.

of 1.2%, and in oil recovery of 4.9%. These discrepancies are small enough to indicate high repeatability. Therefore, Experimental Runs #4 and #6 are not discussed in later sections. All experimental observation results for the CO_2 injection stage are presented in supplementary. Key findings from the experimental runs are summarized in Table 2.

3.1 Pressure difference, net CO_2 stored and oil recovery

This section provides an example of a result at 70 °C and 12 MPa. The pressure difference observed during wsCO_2 injection was higher than that of pure CO_2 (Fig. 3(a)). For pure CO_2, the pressure difference increased sharply before breakthrough (0.22 PVI), then decreased, consistent with previous finding (Saira et al., 2021a). In contrast, for wsCO_2, pressure difference continued to rise, reaching a peak at 0.72 PVI before declining. The increase in pressure difference can be attributed to the greater flow resistance caused by the condensation of water from the wsCO_2, which will be explained later in this section.

wsCO_2 injection showed similar net CO_2 stored and oil recovery compared to pure CO_2 injection. wsCO_2 injection yielded a 1.5% higher ultimate CO_2 stored and a 1.6% higher ultimate oil recovery compared to pure CO_2 injection, as shown in Figs. 3(b) and 3(c). Before CO_2 breakthrough (0.22 PVI), the injected CO_2 displaced an equivalent volume of oil, leading to a linear increase in oil recovery. After breakthrough, oil recovery continuously increased due to the mass transfer between CO_2 and oil at near-miscible conditions (Lake, 1989). The pressure difference at the end of wsCO_2 injection was 7.1 times that for pure CO_2 injection (Fig. 3(a)). Being that wsCO_2 and pure CO_2 have similar properties Table 1, the higher pressure difference observed during wsCO_2 injection should not be attributed to the properties of the fluids.

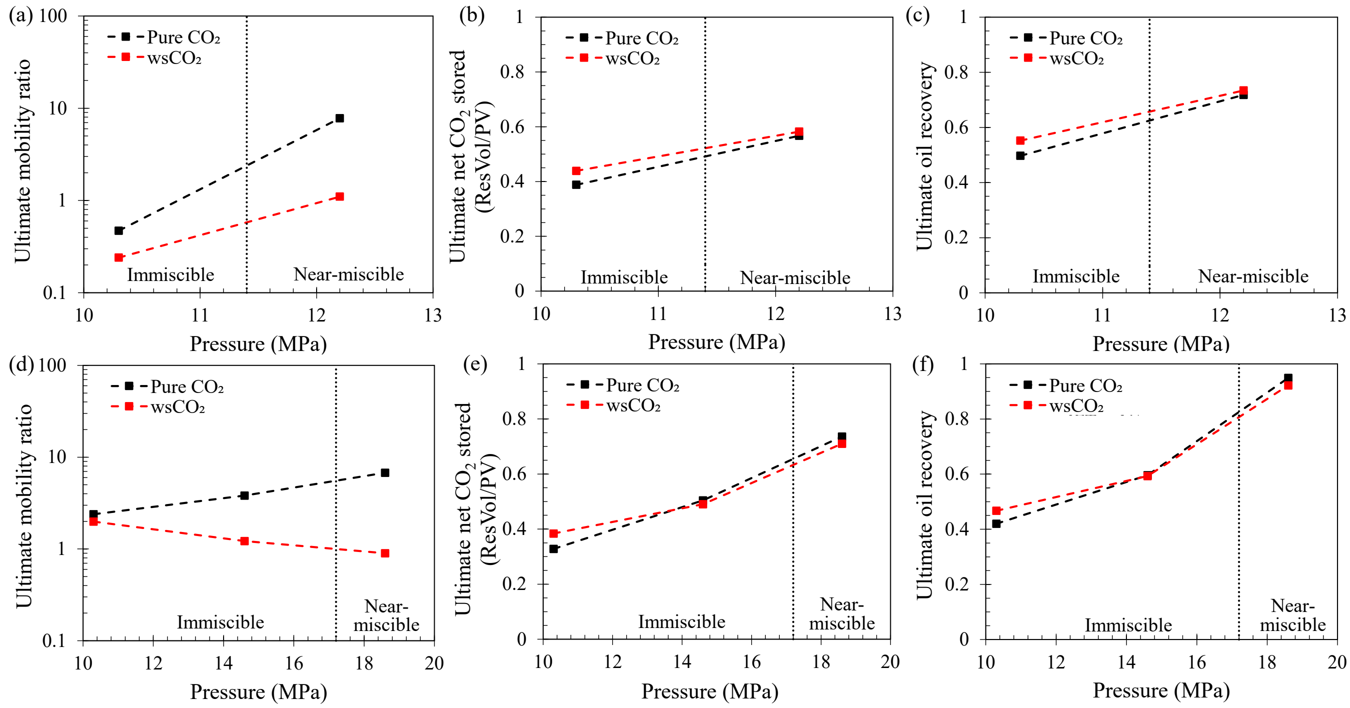

Fig. 4. Ultimate mobility ratio and ultimate oil recovery plotted against experimental pressure under both experimental temperatures. Left: Ultimate mobility ratio at (a) 70 °C and (d) 116 °C. Middle: Ultimate net CO_2 stored at (b) 70 °C and (e) 116 °C. Right: Ultimate oil recovery at (c) 70 °C and (f) 116 °C.

3.2 Mobility reduction results

For pure CO_2 injection at 70 °C, the values of ultimate mobility ratios were 0.47 at 10.3 MPa and 7.8 at 12 MPa (Fig. 4(a)). For pure CO_2 injection at 116 °C, the values of ultimate mobility ratios were 2.4 at 10.3 MPa, 3.8 at 14.6 MPa, and 6.8 at 18.6 MPa (Fig. 4(d)). At higher pressures, miscibility between CO_2 and oil improves, yielding an increase in CO_2 relative permeability and thus a greater mobility ratio (Gong and Gu, 2015; Kamali et al., 2015) as defined in Eq. (4). Increased miscibility is also responsible for better oil displacement; hence, net CO_2 stored and oil recovery increases with pressure. For pure CO_2 injection at 70 °C, ultimate net CO_2 stored was 38.8% at 10.3 MPa and 56.7% at 12 MPa (Fig. 4(b)), and ultimate oil recovery was 49.7% at 10.3 MPa and 71.8% at 12 MPa (Fig. 4(c)). For pure CO_2 injection at 116 °C, ultimate net CO_2 stored was 32.8% at 10.3 MPa, 50.4% at 14.6 MPa, and 73.6% at 18.6 MPa (Fig. 4(e)), and ultimate oil recovery was 42.0% at 10.3 MPa, 59.6% at 14.6 MPa, and 94.9% at 18.6 MPa (Fig. 4(f)).

For $wsCO_2$ injection at 70 °C, ultimate mobility ratios were 0.24 at 10.3 MPa and 1.1 at 12 MPa (Fig. 4(a)). For $wsCO_2$ injection at 116°C, ultimate mobility ratios were 2 at 10.3 MPa, 1.2 at 14.6 MPa, and 0.9 at 18.6 MPa (Fig. 4(d)). The mobility ratio indicates the stability of the displacement front for CO_2 injection. A mobility ratio greater than one indicates that injected CO_2 is more mobile than the displaced oil, thus leading to poor sweep efficiency (Lake, 1989). In contrast, a mobility ratio of nearly or lower than one indicates high sweep efficiency (Dyes et al., 1954; Habermann, 1960). The abovementioned result indicates that $wsCO_2$ improved the ultimate mobility ratio significantly to near one at higher experimental pressures: 12 MPa at 70 °C, and 14.6 and 18.6 MPa at 116 °C. However, at lower experimental pressure (10.3 MPa at 70 and 116 °C), the improvement in ultimate mobility ratio by $wsCO_2$ is limited.

The better $wsCO_2$ mobility control at higher experimental pressure can be explained by water condensation, which is a function of miscibility. During $wsCO_2$ injection, the mixing of CO_2 into the oil causes water to condense into the pore space, resulting in a higher pressure difference yielding a lower mobility ratio (Eq. (4)). However, water condensation depends on experimental pressure: The higher the pressure, the greater the miscibility, causing more CO_2 to mix into the oil (Gu et al., 2013), leading to maximum water condensation. Conversely, at low experimental pressure, there is not enough mass transfer because of the immiscibility. The limited CO_2 mixing into oil results in negligible water condensation, resulting in similar pressure difference and mobility ratio for both CO_2 and $wsCO_2$ injection. Hence, water condensation might not be effective, which would explain why $wsCO_2$ did not lower the mobility ratio at low experimental pressure. Therefore, the ultimate mobility ratio of $wsCO_2$ injection was consistently lower than that of pure CO_2 injection at all experimental temperatures and pressures.

The reduced mobility ratio is governed by the ratio of CO_2 relative permeability to viscosity (Eq. (5)). While the presence of water vapours makes $wsCO_2$ slightly more viscous than pure CO_2 (Table 1), the increase in viscosity is minimal compared to the observed increase in pressure difference observed during $wsCO_2$ injection compared to pure CO_2 injection (Fig.

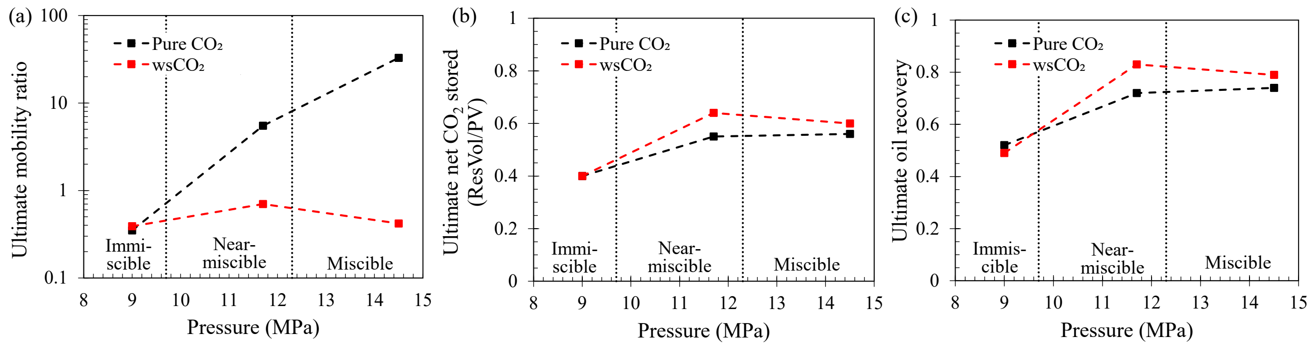

Fig. 5. Literature data on pure CO_2 and wsCO_2 injection at different experimental pressures. All data were obtained at 70 °C: (a) Ultimate mobility ratio, (b) ultimate net CO_2 stored and (c) ultimate oil recovery. (Adapted from Ajoma et al. (2021a).)

Table 3. Coefficients for the exponential relation.

Condition (°C)	A	n
70 (This study)	546	-8.8
116 (This study)	8	-4.5
70 (Ajoma et al., 2021a)	1,684	-10

Notes: Constant coefficient values for the exponential relationship between $M_{wsCO_2}/M_{pure\ CO_2}$ and experimental pressure under different temperatures, as defined in Eq. (8).

3(a)). Therefore, the reduced mobility ratio is primarily attributed to decreased CO_2 relative permeability, and Eq (5). can be used to estimate the reduction.

Like CO_2 injection, the ultimate net CO_2 stored and ultimate oil recovery for wsCO_2 injection increased as the experimental pressure increased. For wsCO_2 injection at 70 °C, ultimate net CO_2 stored was 43.9% at 10.3 MPa and 58.2% at 12 MPa (Fig. 4(b)), and ultimate oil recovery was 55.2% at 10.3 MPa and 73.4% at 12 MPa (Fig. 4(c)). For wsCO_2 injection at 116°C, ultimate net CO_2 stored was 38.4% at 10.3 MPa, 49.0% at 14.6 MPa, and 71.0% at 18.6 MPa (Fig. 4(e)), and ultimate oil recovery was 46.7% at 10.3 MPa, 59.3% at 14.6 MPa, and 92.2% at 18.6 MPa (Fig. 4(f)). Ultimate net CO_2 stored and ultimate oil recovery are dependent on displacement efficiency and sweep efficiency. With the increase of pressure, higher miscibility leads to higher displacement efficiency, and higher mobility ratio leads to lower sweep efficiency (Lake, 1989). At core-scale and under experimental conditions, this work does not observe a significant effect of sweep efficiency. Therefore, the effect of improved mobility ratio is not visible on recovery curves. However, at field-scale, sweep efficiency becomes more influential, as does mobility reduction, also known as mobility control. Therefore, wsCO_2 injection might lead to higher recovery at field-scale.

This work further analyzes the wsCO_2 data presented by Ajoma et al. (2021a). The ultimate mobility ratio, ultimate net CO_2 stored and ultimate oil recovery using wsCO_2 at 70 °C with a mixture of hexane and decane (C_6-C_{10}) vary with pressure, as shown in Fig. 5. Ultimate mobility ratio for pure CO_2 injection was 0.35 at 9 MPa, 5.5 at 11.7 MPa, and 33.9 at 14.5 MPa, whereas mobility ratio for wsCO_2 injection was 0.39, 0.70, and 0.42 at the same pressures (Fig. 5(a)). Ajoma et al. (2021a) observed that wsCO_2 injection yielded additional net CO_2 stored and oil recovery. Ultimate net CO_2 stored for pure CO_2 injection was 0.40 at 9MPa, 0.55 at 11.7 MPa, and 0.56 at 14.5 MPa, whereas net CO_2 stored for wsCO_2 injection was 0.40, 0.64, and 0.60 at the same pressures (Fig. 5(b)). Ultimate oil recovery for pure CO_2 injection was 0.52 at 9 MPa, 0.72 at 11.7 MPa, and 0.74 at 14.5 MPa, whereas ultimate oil recovery for wsCO_2 injection was 0.49, 0.83, and 0.79 at the same pressures (Fig. 5(c)). Thus, Ajoma et al. (2021a) observed that as the pressure increases, wsCO_2 injection becomes more effective at reducing CO_2 mobility and yielding additional net CO_2 stored and oil recovery. In contrast, the lack of improvement in net CO_2 stored and oil recovery observed in this study's experiments could be attributed to differences in the rock and oil used compared to those in Ajoma et al. (2021a).

To further analyze the effectiveness of wsCO_2 injection at reducing CO_2 mobility, Fig. 6 presents the ratio between the ultimate mobility ratio of wsCO_2 (M_{wsCO_2}) and the ultimate mobility ratio of pure CO_2 ($M_{pure\ CO_2}$). A value of $M_{wsCO_2}/M_{pure\ CO_2}$ close to one means that the performance of wsCO_2 would be similar to that of pure CO_2. As $M_{wsCO_2}/M_{pure\ CO_2}$ decreases, the effect of wsCO_2 injection mobility control becomes more pronounced. As pressure increases, the effectiveness of wsCO_2 injection at reducing CO_2 mobility increases. The same data as in Fig. 6(a) are presented in Fig. 6(b), but with the x-axis showing the ratio of pressure to MMP.

A linear relationship is observed between the logarithm of $M_{wsCO_2}/M_{pure\ CO_2}$ and pressure (Fig. 6). The relationship is expressed by:

$$\frac{M_{wsCO_2}}{M_{pure\ CO_2}} = A\exp\left(n\frac{P}{\mathrm{MMP}}\right) \tag{8}$$

where P is the experimental pressure, and A and n are curve fitting parameters. The specific values for A and n under different conditions are summarized in Table 3.

The mobility control effect of wsCO_2 injection at 70 °C was stronger than at 116 °C under the same experimental pressure (Fig. 6(a)). Despite having less effective mobility control, wsCO_2 still achieved one order of magnitude improvement in mobility ratio at the higher temperature and pressure. At high-

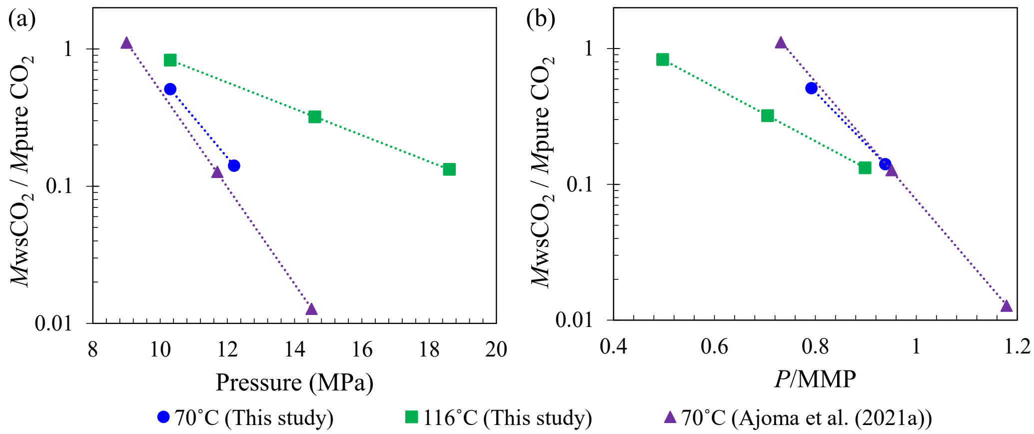

Fig. 6. Semi-logarithmic plot of $M_{wsCO_2}/\ M_{pure\ CO_2}$ versus (a) pressure and (b) P/MMP at different temperatures (70 and 116 °C from this study, and 70 °C from Ajoma et al. (2021a)). Exponential fits are shown for each temperature/study combination.

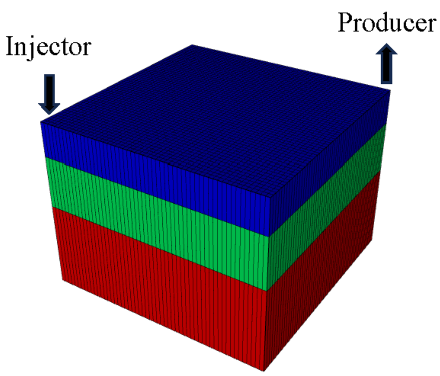

Fig. 7. Reservoir simulation model.

Table 4. Grid information for reservoir simulation model.

Layers	Grid Thickness (m)	K_{ij} (mD)	K_k (mD)
Top	6.1	500	50
Middle	9.1	50	50
Bottom	15.2	200	25

Notes: The grid length and width were uniformly set to 16.8 m. An initial water saturation of 0.23 and a porosity of 0.3 were used for all layers.

er temperatures, CO_2 is less miscible in oil, yielding lower mass transfer (Gu et al., 2013) which explains the weaker mobility control at higher temperature.

To eliminate the influence of differences in miscibility pressure due to different oils and temperature conditions, the x-axis in Fig. 6(b) is expressed as P/MMP. At the same P/MMP-i.e., the same level of miscibility-the mobility control effect of wsCO_2 is stronger at 116 °C than at 70 °C. This contrasts with many other mobility control methods, such as foam injection, which tend to lose effectiveness at higher temperatures. One possible explanation is that the water fraction in wsCO_2 was 0.69-0.73 mol% at 70 °C and 2.7-2.91 mol% at 116 °C, indicating that wsCO_2 holds more water at higher temperatures. This suggests that the mobility control effect of wsCO_2 remains effective across a wide range of pressures and temperatures, particularly under high-pressure high-temperature conditions.

At the same temperature, the relationship between $M_{wsCO_2}/M_{pure\ CO_2}$ and P/MMP remains consistent across different oil samples, indicating that the proposed empirical equation is independent of oil composition (Fig. 6(b)). The exponent n varies with temperature but not with oil composition. However, more experiments are needed to confirm this observation.

4. Numerical simulation

Despite the improved mobility control provided by wsCO_2 injection, experimental observation finds net CO_2 stored and oil recovery to be similar to that of pure CO_2 injection, as CO_2 sweep efficiency is already high in experimental runs. However, at field-scale sweep efficiency is low. To investigate the impact of mobility control on net CO_2 stored at field-scale, this section presents a field-scale numerical simulation.

4.1 Numerical model

This study used a modified SPE-5 model found in Ajoma et al. (2020). The reservoir simulation model and grid information are illustrated in Fig. 7 and Table 4, respectively. Fluid selection and properties are described in Section 2.1. Reservoir conditions were set to 70 °C and 12 MPa to represent near-miscibility. As IFT is negligible at near-miscibility (Fig. 3), capillary pressure was ignored. The fluid properties are detailed in Table 1.

For this simulation, CO_2-oil relative permeability functions were assumed to be linear with respect to saturation. Based on the results from Experimental Runs #3 and #5, k_{ro}^m and $k_{rCO_2}^m$ were calculated using:

$$k_{ro}^m = \frac{q_o \mu_o L}{KA\Delta P_o} \tag{9}$$

$$k_{rCO_2}^m = \frac{q_{CO_2} \mu_{CO_2} L}{KA\Delta P_{CO_2}} \tag{10}$$

where k_{ro}^m was calculated to be 0.64 for both pure CO_2 and wsCO_2 injection. $k_{rCO_2}^m$ were calculated to be 0.2 for

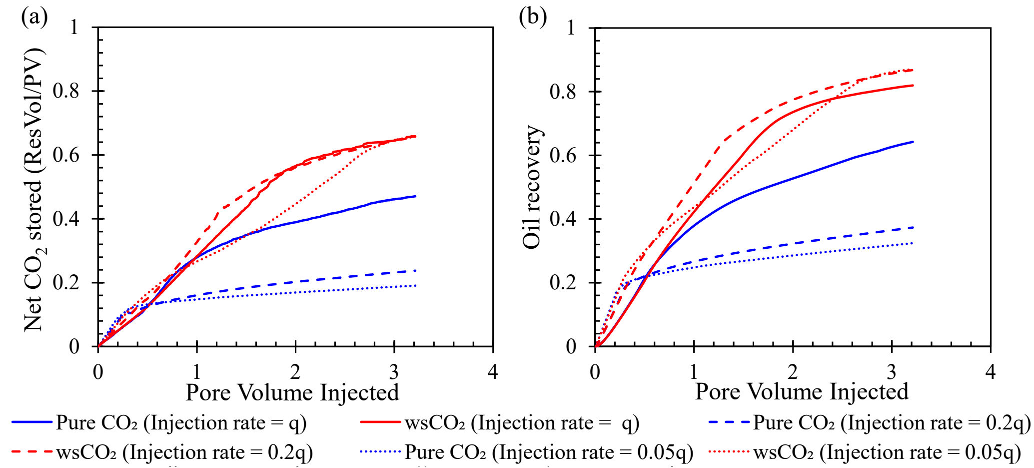

Fig. 8. Simulation results for CO_2 and $wsCO_2$ injection under different injection rate: (a) Net CO_2 stored and (b) oil recovery.

pure CO_2 injection and 0.03 for $wsCO_2$ injection, respectively. Maximum CO_2 saturation was 0.64 in both cases, estimated via material balance. In a realistic scenario, modelling the mixing between $wsCO_2$ and oil would require three-phase (oil–water–vapour) flash calculations. Such condensation could also affect the viscosity of oil phase, particularly if it leads to emulsification (Yin et al., 2025). However, since the objective of the presented simulations is to illustrate the impact of reduced mobility on CO_2 sweep-rather than modelling $wsCO_2$ injection in details-the reduction in relative permeability modeled using Eq. (10) is considered sufficient.

Three injection rates were selected to represent varying gravity effects. The base injection rate (q) was 328,805 m^3/day at surface conditions, following Ajoma et al. (2020). Two additional rates were set at 0.2q and 0.05q. In field-scale simulations, R_l^2 and N_g values indicate that the field-scale simulations are consistent with a gravity dominant flow regime (Zhou et al., 1994).

4.2 Numerical simulation results

Field-scale simulation results for net CO_2 stored are presented in Fig. 8(a). Before breakthrough, net CO_2 stored was a straight line, indicating that all injected CO_2 was stored in the reservoir. For pure CO_2, ultimate net CO_2 stored is greater for higher injection rate, while the injection rate had a minimal effect on ultimate net CO_2 stored for $wsCO_2$ injection. For pure CO_2 injection, the ultimate net CO_2 stored was 47% at q, 24% at 0.2q and 19% at 0.05q. While for $wsCO_2$ injection, the ultimate net CO_2 stored was nearly 66% for all injection rates. Field-scale simulation results for ultimate oil recovery are shown in Fig. 8(b). For pure CO_2 injection, the ultimate oil recovery was 64% at q, 37% at 0.2q and 32% at 0.05q. For $wsCO_2$ injection, the ultimate oil recovery was 82% at q, 87% at 0.2q and 87% at 0.05q.

The ultimate global mole fraction of CO_2 across different layers is presented in Fig. 9. For all simulated injection rates, the top layer was fully swept, which can be attributed to both gravity and permeability promoting the flow of injected fluid in this layer. For pure CO_2 injection, the sweep efficiency in the middle and bottom layers was poor. The middle layer, with its lowest permeability, and the bottom layer, significantly influenced by gravity effect, experienced CO_2 bypassing large portions of these two layers. Additionally, lower injection rates resulted in greater gravity effects, leading to the lowest sweep efficiency for pure CO_2 injection at 0.05q and the highest at q. However, for $wsCO_2$ injection, the sweep efficiency remained between 90-100% for all layers under different injection rates. Overall, by the end of the simulation, net CO_2 stored, oil recovery, and CO_2 sweep efficiency for pure CO_2 injection decreased as the gravity effect increased, while $wsCO_2$ injection was less affected by gravity effect.

The observations in Figs. 8 and 9 can be explained by greater mobility control during $wsCO_2$ injection. The values of mobility ratios for pure CO_2 and $wsCO_2$ injection were 7.8 and 1.1, respectively, indicating that $wsCO_2$ injection achieved a higher sweep efficiency than pure CO_2 injection.

At lower injection rates, gravity plays a more significant role, causing the injected CO_2 to bypass more space compared to higher injection rates. As a result, the net CO_2 stored and oil recovery for pure CO_2 injection were higher at high injection rates and lower at low injection rates. However, the loss of net CO_2 stored and oil recovery due to the gravity effect can be mitigated by the lower mobility ratio during $wsCO_2$ injection.

As previously noted, accurately modeling $wsCO_2$ injection requires complex numerical frameworks. A more tractable alternative is to apply analytical approaches based on self-similar solutions for near-miscible 1D oil displacement (Lake, 1989). These solutions can be derived using splitting methods for multicomponent systems (Borazjani et al., 2016). Furthermore, classical methods such as Welge and JBN can be generalized using self-similarity principles without requiring the full solution (Borazjani et al., 2019). Incorporating splitting techniques could enhance the estimation of relative permeability and EoS parameters from laboratory data, such as those used in this study.

5. Conclusions

The paper proposes $wsCO_2$ injection as a solution for CO_2 storage challenges in high-pressure high-temperature reservoirs. Injection experiments were conducted on Bentheimer

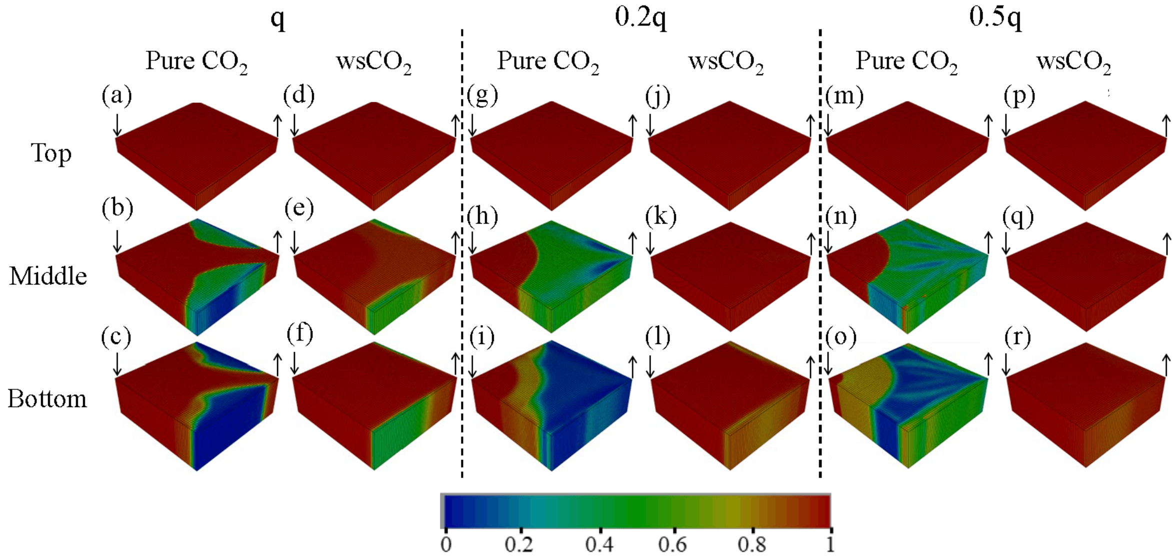

Fig. 9. Ultimate global mole fraction of CO_2 across different layers (Top, Middle, Bottom) for various injection rates (q, 0.2q, 0.5q) comparing pure CO_2 and wsCO_2 injections. The top row shows that the first layer was fully swept with both pure CO_2 and wsCO_2 injections across all injection rates ((a), (d), (g), (j), (m), (p)). In the middle row, sweep efficiency decreased due to low permeability during pure CO_2 injection ((b), (h), (n)). In the bottom row, sweep efficiency was reduced due to the gravity effect in pure CO_2 injection ((c), (i), (o)). However, for wsCO_2 injections in the middle and bottom layers, the sweep efficiency remained between 90%-100% across all injection rates ((e), (k), (q), (f), (l), (r)).

sandstone cores, and the results of wsCO_2 injection are compared against those of pure CO_2 injection. Based on the experimental results, the following conclusions can be drawn:

1) wsCO_2 injection provides effective mobility control for both low- and high-temperature reservoirs, particularly under high-pressure conditions. Although mobility control is somewhat weaker at higher temperatures, this is attributed to the increased miscibility pressure at elevated temperatures.
2) A strong correlation (Eq. (8)) was found between wsCO_2 mobility control effectiveness and normalized pressure (P/MMP), with improved performance at higher pressures. Additionally, at the same P/MMP – i.e., the same level of miscibility – wsCO_2 showed stronger mobility control at 116 °C than at 70 °C. Since pure CO_2 sweep efficiency is poorest under high-pressure high-temperature conditions (Bedrikovetsky, 1993), wsCO_2 becomes especially effective when mobility control is most needed, enhancing its potential for CO_2 storage in deep reservoirs.
3) The experimental results suggest that the empirical fitting parameters are not sensitive to oil composition. However, more experiments are needed to confirm this observation.
4) Although wsCO_2 injection did not significantly improve net CO_2 stored and oil recovery in the experimental observations of this study due to the already high CO_2 sweep efficiency in the laboratory, it showed improvements in the field-scale simulations conducted in this study, with a 19%-47% increase in net CO_2 stored and an 18%-55% increase in oil recovery.

Conventional mobility control methods, such as CO_2-WAG injection and CO_2-SWAG injection, either reduce CO_2 storage, while other methods, such as CO_2 foam injection, only work at certain pressures and temperatures. Previous work has shown that wsCO_2 injection yields CO_2 storage much greater than CO_2-WAG injection and CO_2-SWAG injection, as injected water during CO_2-WAG injection and CO_2-SWAG injection restricts the available pore space for CO_2 storage (Ajoma et al., 2021b). In conclusion, wsCO_2 injection represents a more sustainable alternative for oil recovery and CO_2 storage, combining effective mobility control with broad operational flexibility across diverse reservoir conditions.

Acknowledgements

The authors thank David Levin for his assistance with language editing. Hang Yin gratefully acknowledges support from the Australian Government Research Training Program (RTP) Scholarship.

Supplementary file

https://doi.org/10.46690/ager.2025.06.07

Conflict of interest

The authors declare no competing interest.

References

Abdelaal, A., Gajbhiye, R., Al-Shehri, D. Mixed CO_2/N_2 foam for eor as a novel solution for supercritical CO_2 foam challenges in sandstone reservoirs. ACS Omega, 2020, 5(51): 33140-33150.

Ajoma, E., Saira, Sungkachart, T., et al. Water-saturated CO_2 injection to improve oil recovery and CO_2 storage. Applied Energy, 2020, 266: 114853.

Ajoma, E., Saira, Sungkachart, T., et al. Effect of miscibility and injection rate on water-saturated CO_2 injection. Energy, 2021a, 217: 119391.

Ajoma, E., Sungkachart, T., Saira, et al. A laboratory study of coinjection of water and CO_2 to improve oil recovery and CO_2 storage: Effect of fraction of CO_2 injected. SPE Journal, 2021b, 26(4): 2139-2147.

Arshad, A., Al-Majed, A. A., Menouar, H., et al. Carbon dioxide (CO_2) miscible flooding in tight oil reservoirs: A case study. Paper SPE 127616 Presented at the Kuwait International Petroleum Conference and Exhibition, Kuwait City, Kuwait, 14-16 December, 2009.

Bedrikovetsky, P. Mathematical Theory of Oil and Gas Recovery: With Applications to Ex-ussr Oil and Gas Fields. Springer Science & Business Media, 1993.

Bello, A., Ivanova, A., Cheremisin, A. Enhancing N_2 and CO_2 foam stability by surfactants and nanoparticles at high temperature and various salinities. Journal of Petroleum Science and Engineering, 2022, 215: 110720.

Bloomfield, V. A., Dewan, R. K. Viscosity of liquid mixtures. The Journal of Physical Chemistry, 1971, 75(20): 3113-3119.

Borazjani, S., Behr, A., Genolet, L., et al. Ion-exchange inverse problem for low-salinity coreflooding. Transport in Porous Media, 2019, 128(2): 571-611.

Borazjani, S., Roberts, A. J., Bedrikovetsky, P. Splitting in systems of pdes for two-phase multicomponent flow in porous media. Applied Mathematics Letters, 2016, 53: 25-32.

Cao, C., Liu, H., Hou, Z., et al. A review of CO_2 storage in view of safety and cost-effectiveness. Energies, 2020, 13(3): 600.

Chen, H., Wei, B., Zhou, X., et al. Theory and technology of enhanced oil recovery by gas and foam injection in complex reservoirs. Advances in Geo-Energy Research, 2025, 15(3): 181-184.

Chen, Y., Elhag, A. S., Worthen, A. J., et al. High temperature CO_2-in-water foams stabilized with cationic quaternary ammonium surfactants. Journal of Chemical & Engineering Data, 2016, 61(8): 2761-2770.

Clark, J. A., Santiso, E. E. Carbon sequestration through CO_2 foam-enhanced oil recovery: A green chemistry perspective. Engineering, 2018, 4(3): 336-342.

CMG-WINPROP. Winprop (version 2018). Calgary, Canada: Computer Modelling Group Ltd., 2018.

Dyes, A. B., Caudle, B. H., Erickson, R. A. Oil production after breakthrough as influenced by mobility ratio. Journal of Petroleum Technology, 1954, 6(4): 27-32.

El-Dessouky, E. Appendix A-Thermodynamic properties, in Fundamentals of Salt Water Desalination, edited by Hisham T. El-Dessouky and Hisham M. Ettouney, Elsevier, Amsterdam, pp. 525-563, 2002.

Emrani, A. S., Nasr-El-Din, H. A. An experimental study of nanoparticle-polymer-stabilized CO_2 foam. Colloids and Surfaces A: Physicochemical and Engineering Aspects, 2017, 524: 17-27.

Ge, J., Saira, Smith, B., et al. Laboratory comparison of tertiary N_2, CH_4, and CO_2 injection into an inland oil field sample. Fuel, 2022, 324: 124635.

Gong, Y., Gu, Y. Miscible CO_2 simultaneous water-and-gas (CO_2-SWAG) injection in the bakken formation. Paper SPE 175976 Presented at the SPE/CSUR Unconventional Resources Conference, Calgary, Alberta, Canada, 20-22 October, 2015.

Grabowski, A., Nercessian, O., Fayolle, F., et al. Microbial diversity in production waters of a low-temperature biodegraded oil reservoir. FEMS Microbiology Ecology, 2005, 54(3): 427-443.

Gu, Y., Hou, P., Luo, W. Effects of four important factors on the measured minimum miscibility pressure and first-contact miscibility pressure. Journal of Chemical & Engineering Data, 2013, 58(5): 1361-1370.

Habermann, B. The efficiency of miscible displacement as a function of mobility ratio. Transactions of the AIME, 1960, 219(1): 264-272.

Kamali, F., Hussain, F. Field-scale simulation of CO_2 enhanced oil recovery and storage through SWAG injection using laboratory estimated relative permeabilities. Journal of Petroleum Science and Engineering, 2017, 156: 396-407.

Kamali, F., Hussain, F., Cinar, Y. A laboratory and numerical-simulation study of co-optimizing CO_2 storage and CO_2 enhanced oil recovery. SPE Journal, 2015, 20(6): 1227-1237.

Kamali, F., Hussain, F., Cinar, Y. An experimental and numerical analysis of water-alternating-gas and simultaneous-water-and-gas displacements for carbon dioxide enhanced oil recovery and storage. SPE Journal, 2017, 22(2): 521-538.

Kim, S., Santamarina, J. C. Engineered CO_2 injection: The use of surfactants for enhanced sweep efficiency. International Journal of Greenhouse Gas Control, 2014, 20: 324-332.

Kulkarni, M. M., Rao, D. N. Experimental investigation of miscible and immiscible water-alternating-gas (WAG) process performance. Journal of Petroleum Science and Engineering, 2005, 48(1-2): 1-20.

Kumar, N., Sampaio, M. A., Ojha, K., et al. Fundamental aspects, mechanisms and emerging possibilities of CO_2 miscible flooding in enhanced oil recovery: A review. Fuel, 2022, 330: 125633.

Kumar, S., Mandal, A. A comprehensive review on chemically enhanced water alternating gas/CO_2 (cewag) injection for enhanced oil recovery. Journal of Petroleum Science and Engineering, 2017, 157: 696-715.

Lake, L. W. Enhanced Oil Recovery. Old Tappan, USA, Prentice Hall Inc., 1989.

Liu, M. K., Andrianov, A. I., Rossen, W. R. Sweep efficiency in CO_2 foam simulations with oil. Paper SPE 142999 Presented at the SPE EUROPEC/EAGE Annual Conference and Exhibition, Vienna, Austria, 23-26 May, 2011.

Lv, Q., Zhou, T., Luan, Y., et al. A green aqueous foam stabilized by cellulose nanofibrils and camellia saponin for geological CO_2 sequestration. Journal of Cleaner Production, 2023, 406: 136980.

Orr, F. M., Jessen, K. An analysis of the vanishing interfacial tension technique for determination of minimum miscibility pressure. Fluid Phase Equilibria, 2007, 255(2): 99-109.

Perera, M. S. A., Gamage, R. P., Rathnaweera, T. D., et al. A review of CO_2-enhanced oil recovery with a simulated sensitivity analysis. Energies, 2016, 9(7): 481.

Puerto, M., Hirasaki, G. J., Miller, C. A., et al. Surfactant systems for EOR in high-temperature, high-salinity environments. SPE Journal, 2011, 17(1): 11-19.

Saira, Ajoma, E., Le-Hussain, F. A laboratory investigation of the effect of ethanol-treated carbon dioxide injection on oil recovery and carbon dioxide storage. SPE Journal, 2021a, 26(5): 3119-3135.

Saira, Janna, F., Le-Hussain, F. Effectiveness of modified CO_2 injection at improving oil recovery and CO_2 storage-review and simulations. Energy Reports, 2020a, 6: 1922-1941.

Saira, Yin, H., Le-Hussain, F. Effect of alcohol-treated CO_2 on interfacial tension between CO_2 and oil, and oil swelling. Advances in Geo-Energy Research, 2021b, 5(4): 407-421.

Saira, S., Yin, H., Le-Hussain, F. Using alcohol-treated CO_2 to reduce miscibility pressure during CO_2 injection. Paper SPE 202341 Presented at Paper presented at the SPE Asia Pacific Oil & Gas Conference and Exhibition, Virtual, 17-19 November, 2020b.

Schneider, C. A., Rasband, W. S., Eliceiri, K. W. NIH Image to ImageJ: 25 years of image analysis. Nature Methods, 2012, 9(7): 671-675.

Shyeh-Yung, J-G. J. Mechanisms of miscible oil recovery: Effects of pressure on miscible and near-miscible displacements of oil by carbon dioxide. Paper SPE 22651 Presented at the SPE Annual Technical Conference and Exhibition, Dallas, Texas, 6-9 October, 1991.

Thomas, F. B., Holowach, N., Zhou, X., et al. Miscible or near-miscible gas injection, which is better? Paper SPE 27811 Presented at the SPE/DOE Improved Oil Recovery Symposium, Tulsa, Oklahoma, 17-20 April, 1994.

Yin, H., Ge, J., Cook, B., et al. Tertiary oil recovery and CO_2 storage from laboratory injection of CO_2 or water-saturated CO_2 into a sandstone core. International Journal of Coal Geology, 2023, 275: 104300.

Yin, H., Ge, J., Tung, P. K. M., et al. Water-saturated CO_2 injection in a carbonate rock-effect of pore heterogeneity. Marine and Petroleum Geology, 2025, 173: 107260.

Zhao, F., Hao, H., Hou, J., et al. CO_2 mobility control and sweep efficiency improvement using starch gel or ethylenediamine in ultra-low permeability oil layers with different types of heterogeneity. Journal of Petroleum Science and Engineering, 2015, 133: 52-65.

Zhou, D., Fayers, F. J., Orr, F. M., Jr. Scaling of multiphase flow in simple heterogeneous porous media. Paper SPE 27833 Presented at the SPE/DOE Improved Oil Recovery Symposium, Tulsa, Oklahoma, 17-20 April, 1994.

Zhou, X., Yu, W., Lei, G., et al. Experimental study on dual benefits of improvement of CO_2 enhanced oil recovery and its storage capacity for depleted carbonate oil reservoirs. Advances in Geo-Energy Research, 2024, 12(1): 52-65.

Zou, S., Hussain, F., Arns, J., et al. Computation of relative permeability from *in-situ* imaged fluid distributions at the pore scale. SPE Journal, 2018, 23(3): 737-749.